CERN - EUROPEAN ORGANIZATION FOR NUCLEAR RESEARCH

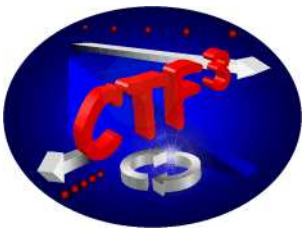

CTF3-Note-094

Data Analysis for PETS Recirculation

V. Ziemann
Department of Physics and Astronomy
Uppsala University

Abstract

We discuss a simple algorithm that determines the PETS recirculation phase and gain as a function of time along the electron beam pulse from measurements at an IQ-detector. Furthermore, even the coupling of the beam to the RF and the phase between the PETS and the detector can be resolved. In the process we find that there is a significant variation of the recirculation gain and phase along the pulse, part of which might be attributable to instrumental non-linearities in the IQ-detectors. Investigating a pulse with breakdown shows a dropping recirculation gain and a linear phase shift following the discharge.

Geneva, Switzerland

March 15, 2009

1 Introduction

In Ref. [1] we discussed a simple model that describes the power recirculation in the PETS structures that are currently being tested in the Two-beam Test-Stand in CTF3 at CERN [2, 3]. A schematic sketch of the recirculation method is depicted in Fig. 1, where the beam generates the RF power of which a fraction is recirculated back to the input coupler after a part is split off for power and IQ detectors and passes through a phase shifter. We used this model with constant recirculation gain g, taking into account the power splitting and losses in the system and the phase ϕ which takes into account variations in the round-trip time of the RF power. The agreement between measured and simulated power signals was quite satisfactory, but the agreement of fitted IQ-signals to measured signals was poor, indicating that there is physics at work beyond the simple assumption of a constant recirculation gain and phase. In this note will derive an algorithm that determines the variation of the two parameters along the beam pulse.

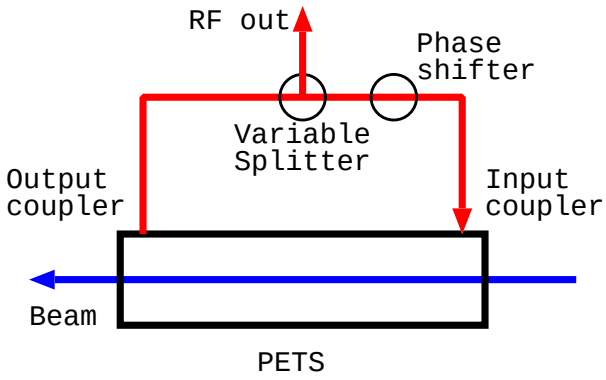

Figure 1: Schematics of the recirculation mechanism. Note that the measurement windows are at the output coupler and at the RF-out port.

2 The Algorithm

In the following we label the (real-valued) coupling between the beam current I_m by a such that the field in the cavity after one round-trip time $\tau = 26\,\text{ns}$ is given by [4]

$$E_m = aI_m + q_m E_{m-1} \tag{1}$$

where the index m labels time in units of round-trip time periods. Here $q_m = g_m e^{i\phi_m}$ is the recirculation gain and phase after the bunch at "time" m has passed wheras In Ref. [4] the q_m were considered constant. E_m is the complex field present in the PETS while bunch m is also present in the PETS. In this way we can calculate the field E_m as a function of "time" m. We verified that the RF power profile for a given BPM intensity profile agrees exactly with that generated by the method in Ref. [1].

Conversely, we can assume that we can measure the beam current I_m and the field E_m as a function of "time" m and solve for the complex recirculation gain q_m, also as a function of "time" and arrive at

$$q_m = \frac{E_m - aI_m}{E_{m-1}} \ . \tag{2}$$

The assumption, however, that we can measure the field E_m inside the PETS is not quite correct. Instead we can measure it somewhere after the beam power splitter shown in Fig 1 at a point that has an unknown phase relation to the reference point inside the PETS. The observable quantities $\bar{E}$ are thus

$$\bar{E} = e^{i\psi} E \ . \tag{3}$$

where the unknown phase is denoted by ψ. Rewriting eq. 2 in terms of the observable fields $\bar{E}$ we find

$$q_m = \frac{e^{-i\psi}\bar{E}_m - aI_m}{e^{-i\psi}\bar{E}_{m-1}} = \frac{\bar{E}_m - ae^{i\psi}I_m}{\bar{E}_{m-1}} \ . \tag{4}$$

Note that an intensity difference between the measured fields $\bar{E}$ and field E in PETS can be easily taken into account by modifying the coupling a. We now face the problem that we do neither know a nor ψ and have to determine them by other means. To this end we observe that a and ψ are are constant for a given experimental setup or at least more slowly varying than the recirculation gain and phase in q_m. We can therefore determine the generalized coupling $c = ae^{i\psi}$ by minimizing the variation χ^2 of the q_m which we define by

$$\chi^2 = \frac{1}{M}\sum_{m=1}^{M}(q_m - \bar{q})^2 \tag{5}$$

where we have introduced the mean $\bar{q}$ by

$$\bar{q} = \frac{1}{M}\sum_{m=1}^{M} q_m \ . \tag{6}$$

Note that this minimization procedure yields as fit results the real and imaginary part of $c = ae^{i\psi}$, which means that the absolute value describes the coupling of the electron beam to the electric field in the PETS as is shown in eq. 1 and the previously unknown phase between the PETS and the IQ-detector. Especially the dependence of the coupling a to parameter variations such as orbit in the PETS will be a useful quantity in the experimental optimization of the power generation.

3 Testing the Algorithm

In order to test the algorithm we generate data by generating synthetic data using the programs described in ref. [1]. We start with a BPM pulse that extends from 100 to 250 ns, has the current of 3 A and the recirculation time, gain, and phase are 26 ns, 0.8

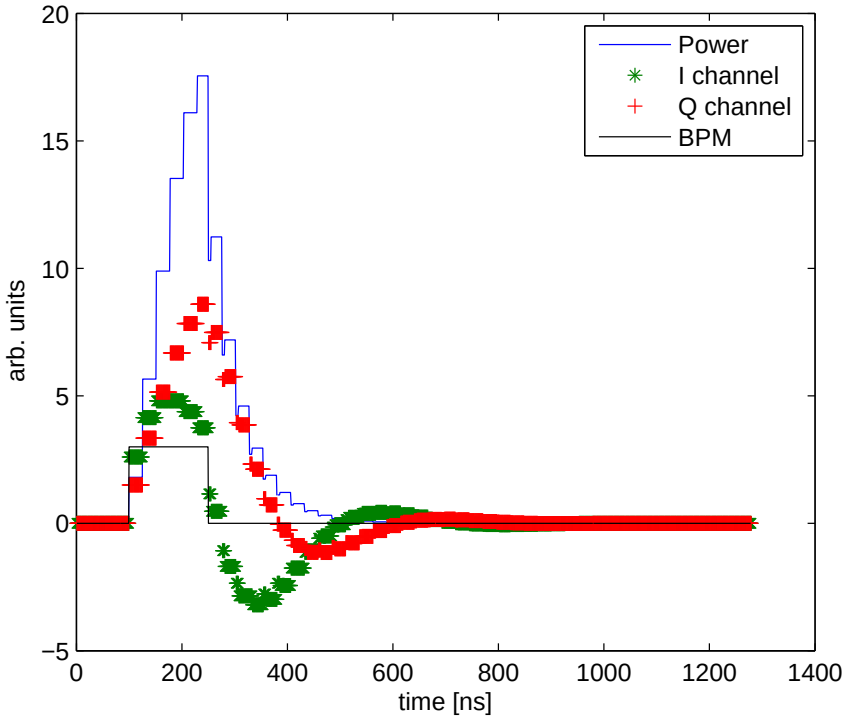

Figure 2: The power and IQ channels of the synthetically generated RF pulse with parameters described in the text.

and 20 degree, respectively. For the coupling we chose $a = 1$ and the phase between the PETS and the IQ detector is $\psi = 30$ degree. The simulated pulse and IQ-signals are shown in Fig. 2.

The IQ channels are then subjected to the analysis described above, i.e. we use Matlab [5] to calculate the q_m along the pulse, whenever the electric field `Ebar` is larger than 10 % of its maximum value, according to

```
Ebar=chI+ichQ;
c=x(1)+i*x(2);
cut=0.1*max(abs(Ebar));
q=zeros(1,length(Ebar));
for j=ktime+1:length(Ebar)
   if abs(Ebar(j-ktime))>cut
       q(j)=(Ebar(j)-c*II(j))/Ebar(j-ktime);
   end
end
```

where `Ebar=chI+i*chQ` is the complex electric field at the IQ-detector, constructed from the measured values `chI` and `chQ` if the detector. Moreover, `ktime` is the recirculation

time in sampling units and `II` contains the BPM pulse. Note that we use two real variables `x(1)` and `x(2)` to construct the imaginary quantity `c` that is later used to minimize the variance of `q` whenever the recirculation gain `abs(q)` is larger than 0.05.

Running the recovery algorithm on the synthetic data returns the input values $a = 1$ and $\psi = 30$ degree exactly. Figure 3 shows contour and surface plots of the cost-function χ^2 versus the fit parameters a and ψ. We observe that the minimum is well defined and corresponds to the correct values $a = 1$ and $\psi = 30$ degrees. Once the unknown coupling a and ψ are known the recirculation parameters q_m can be determined from eq. 4 and plotted along the beam pulse as long as there is sufficient signal strength in the IQ signals. The resulting recirculation gain abs(q_m) and phase arg(q_m) are shown in Fig. 4 and we find that the values for the recirculation parameters $g = 0.8$ and $\phi = 20$ degree are perfectly recovered.

The robustness of the method can be checked by adding noise to the bpm and IQ-channels. We added equally distributed random numbers in the range ± 0.5 to the IQ-channels and ± 0.25 to the bpm data and ran the reconstruction algorithm once again. On the left side of Fig. 6 we show the signals with noise added. In Fig. 5 we show the contour and surface plots for the cost-function χ^2 and find that the surface becomes more shallow, which makes the definition of the minimum less pronounced. This will exhibit itself as a larger uncertainty in the reconstructed fit parameters a and ψ. In this case the reconstructed values are $a = 1.04$ and $\psi = 30.7$ degree. Using these fit parameters we can reconstruct the recirculation parameters q_m according to eq. 4 and display the corresponding gain and phase on the right in Fig. 6 together with a 21-point smoothed average in red. Here we observe that the reconstruction still works but the reconstructed gain and phases vary by a few percent.The result is approximately correct while the power in sufficiently large but during the decaying phase the reconstruction becomes meaningless.

In order to establish the scaling of the error bars of the reconstructed phases with errors in the current measurement of the BPM and the measurements of the IQ detectors we run the simulation with selected random errors and calculate the rms of the reconstructed recirculation gain and phase in the range from 150 to 400 ns and plot the mean value and the RMS versus the RMS BPM and IQ errors. The result is shown in Fig. 7 where we observe that we can tolerate RMS BPM errors of 0.1 A which needs to be compared to the maximum current of 3 A. Similarly the error of the IQ detector is on the order of 0.1 compared to the maximum signal of about 10 that is visible in Fig. 2. We conclude that we can tolerate a few percent random errors in the BPM current measurements and only about 1 percent in the measurements of the IQ detector, which appears rather tight. But, on the other hand, inspection of the measured signals in the top left of Fig. 8 shows that the noise level of the recorded BPM and IQ signals is rather low.

After having established and tested the algorithm we now start to apply it to the measured data that was already used in ref. [1].

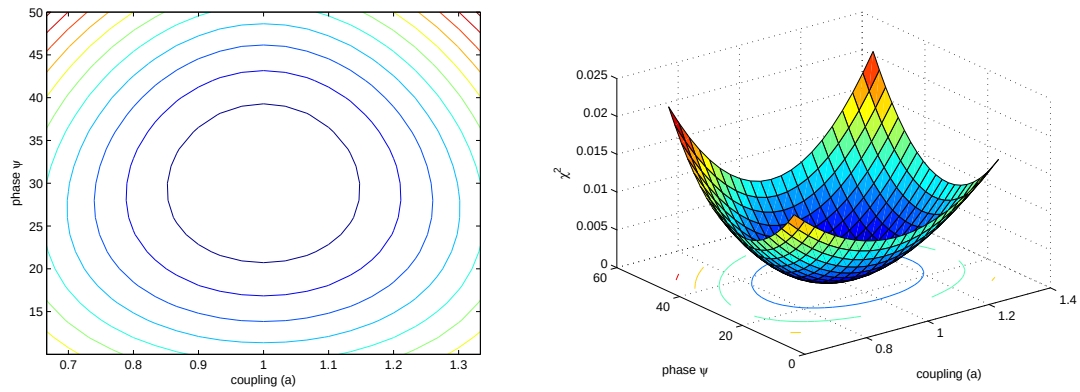

Figure 3: Contour and surface plots of the χ^2 function as a function of the fit parameters coupling a and phase ψ which both were reproduced in the fit correctly to $a = 1$ and $\psi = 30$ degree.

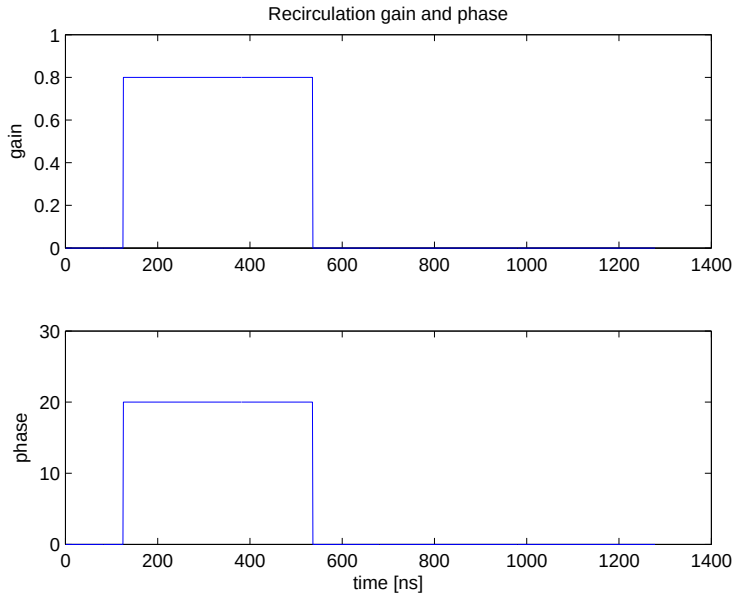

Figure 4: The reconstructed recirculation gain and phase.Note that the reconstruction works well after the bpm pulse has ended at 250 ns.

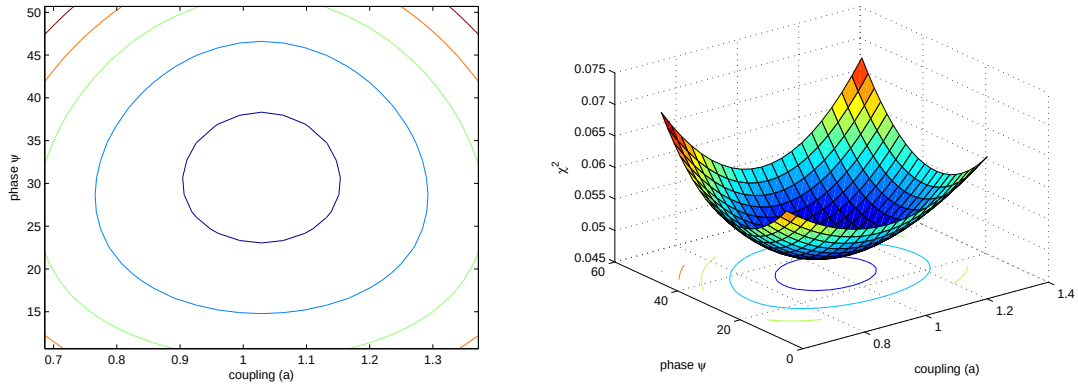

Figure 5: In this case the IQ-channels are perturbed by an equally distributed random signal in the range ± 0.5 and the BPM signal ± 0.25. In this case the minimum becomes more shallow and the definition of the minimum is less well-defined. However the minimum was determined to be at a coupling of $a = 1.04$ and $\psi = 30.7$ degree

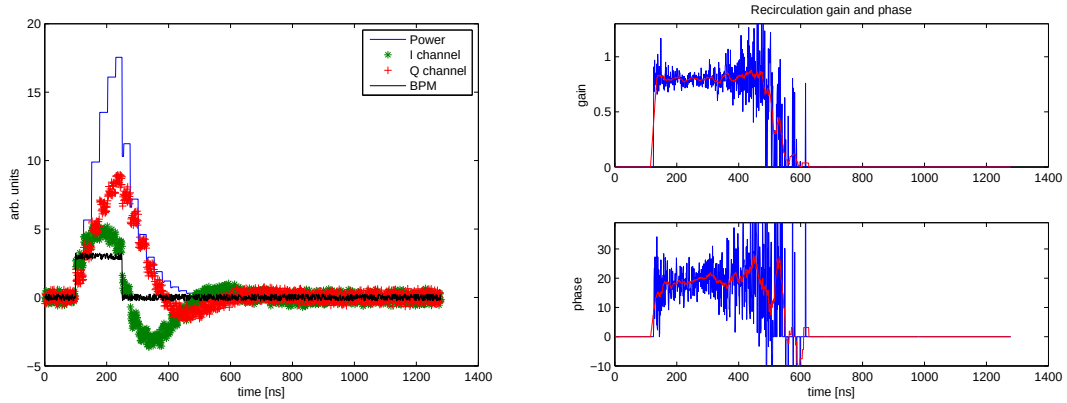

Figure 6: The reconstructed recirculation gain and phase. Here the reconstruction works reasonably well while the IQ signals are large but deteriorates when they become small.

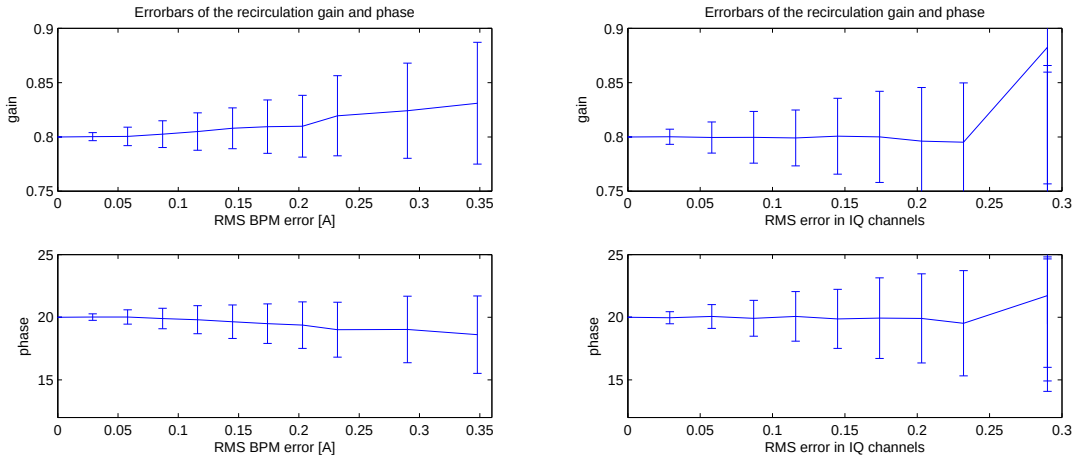

Figure 7: The average value and error bars for the recirculation gain and phase on the flat top between 150 and 400 ns for varying RMS BPM errors (left) and IQ detector errors (right).

4 Measurements

We will use the same measured data from Nov. 28 2008 used in Ref. [1] that exhibited poor agreement between the measured and reconstructed IQ data and subject it to the analysis discussed in the previous section. The input data are shown in the top left corner of Fig. 8 where the upper section displays the BPM intensity and the RF power pulse, respectively and the lower section the recorded IQ-channels. Here we have shifted the raw data in time in order to synchronize them and also subtracted an offset such that the data are close to zero outside the pulse.

We then use the minimization of the χ^2 in Eq. 5 to determine the coupling a of the beam to the fields in the PETS and the phase ψ between PETS and IQ-detector. The values returned here are $a = 7 \times 10^{-3}$ and $\psi = 87°$. The robustness of the fit is illustrated by the variation of the χ^2 around the minimum that is shown in the two plots at the upper right of Fig. 8. the contour-plot shows iso-χ^2 lines around the fitted values and the surface plot below visualizes the variation of the magnitude of the χ^2. Since we have a well-defined minimum we conclude that the fit is robust. In the process of performing the fit the recirculation parameters q_m from eq. 4 are determined. In the middle left of Fig. 8 we show the magnitude and phase of the thus reconstructed q_m in blue together with a 21-point smoothed average in red. Note that at the start of the pulse we only start fitting after the IQ-channels have reached a sufficiently large non-zero value in order to avoid excessive noise in the data. Observing the plots for gain and phase it is remarkable that the values vary smoothly, but they are not constant, as was assumed in Ref. [1].

We can now use the reconstructed values of the recirculation parameter q_m, the coupling a and the phase ψ to calculate the IQ parameters from the BPM pulse and compare

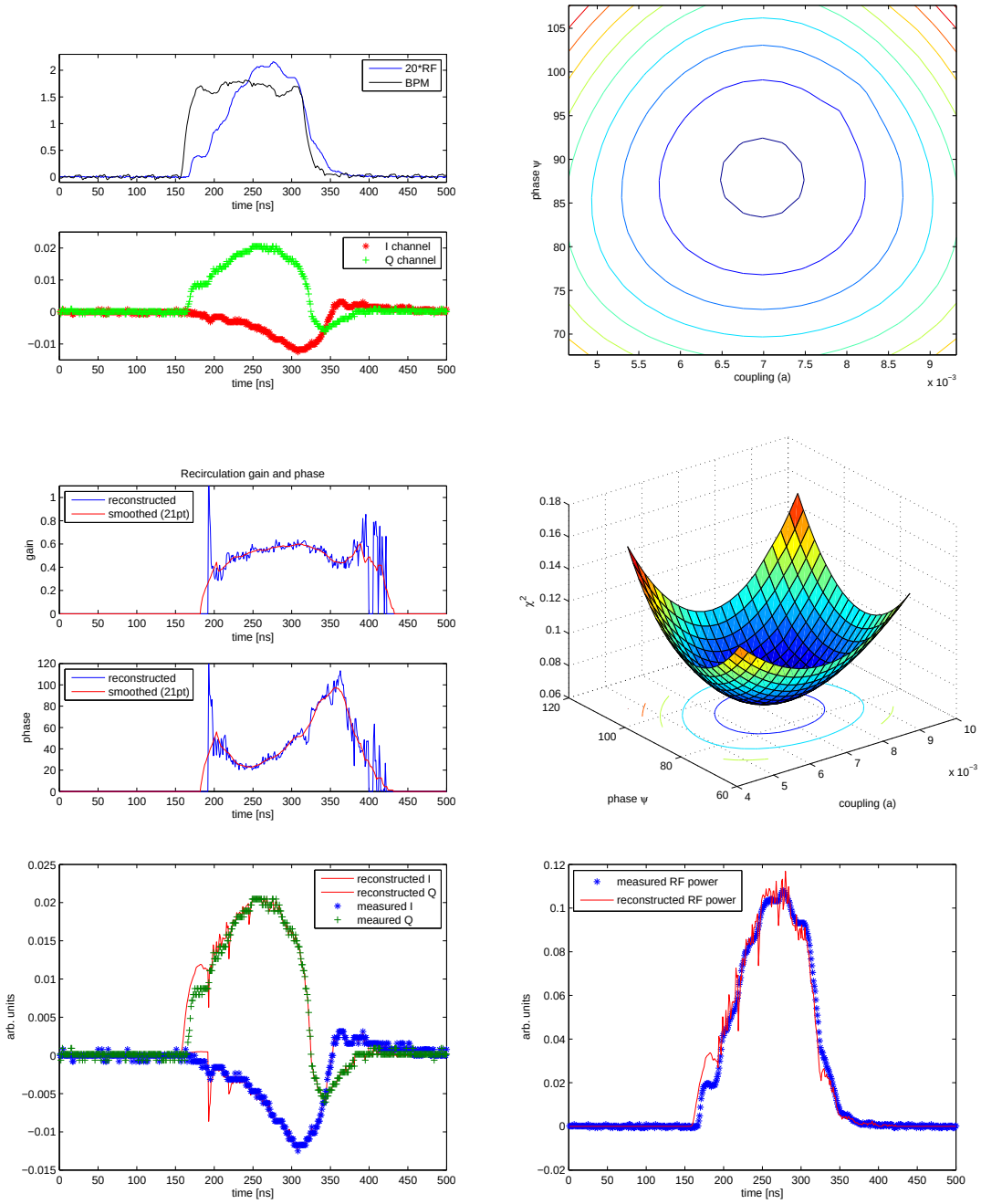

Figure 8: Data from Nov 28, 2008. The measured input signals used in the reconstruction algorithm are shown in the top left plot and the two top plots on the right show the χ^2 versus coupling and phase ψ surfaces, that define the accuracy of the fit as discussed in the text. The plot in the middle left displays the time dependence of the reconstructed recirculation gain and phase. The bottom row displays the reconstructed IQ signals overlayed on the measured and the power profile.

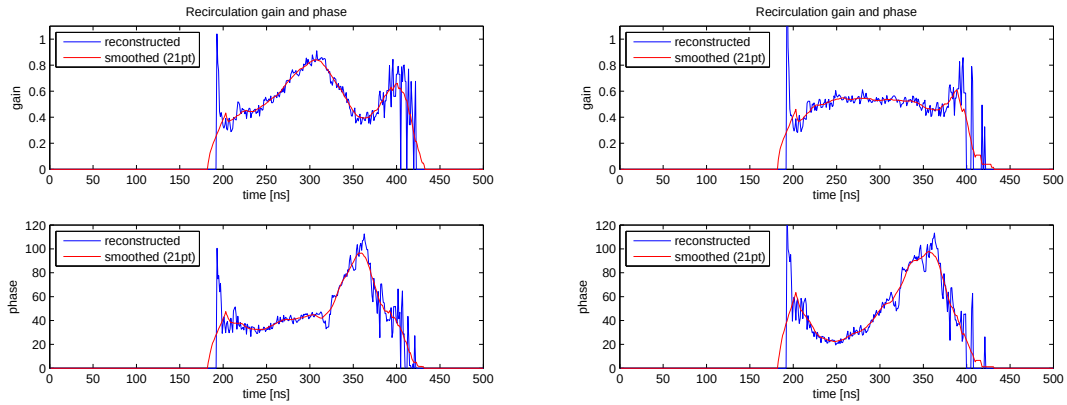

Figure 9: The magnitude and phase of the recirculation parameters with positive (left) and negative (right) non-linearity. Compare these plots to that in the center left of Fig. 8.

with the measured IQ parameters in order to check the consistency of the reconstructed parameters. The calculation of the IQ parameters is done in the following way

```
E(1:ktime)=0;
for m=ktime+1:length(bpm)
    E(m)=a*bpm(m)+q(m)*E(m-ktime);
end
E=exp(i*psi*degree)*E;
I=real(E);
Q=imag(E);
```

where `ktime` is the recirculation time, here 26 ns. We see that this just represents the straightforward application of Eq. 1 with the BPM intensity in the array `bpm` and the electric field `E` representing the I and Q channels. The plot at the lower left in Fig. 8 shows the measured I and Q data in blue and green and the reconstructed data as a red curve. The agreement is quite remarkable. We can then also use the reconstructed IQ signals and derive the power signal, which can in turn be compared with the measured power signal. After re-scaling the magnitude, the measured and reconstructed power signal are shown in the lower right of Fig. 8. Again, with remarkable agreement.

The significant phase and gain variation of the recirculation parameter is quite surprising and one might suspect some non-linearity in the IQ detector to be the culprit. In order to investigate this we rescaled the measured IQ data in `chI` and `chQ` in the following way

```
fudge=8;   % parameter for non-linearity
chI=chI-fudge*(chI+0.03).^2+fudge*0.03^2;
chQ=chQ-fudge*(chQ+0.03).^2+fudge*0.03^2;
```

which basically adds a quadratic non-linearity whose magnitude is controlled by the parameter `fudge`. The offset by -0.03 which is below the smallest value makes sure that all values are affected by the same curvature. The last term make sure that the zero of the curves is not affected. With `fudge=0` the results are identical to those displayed in Fig. 8.

Redoing the reconstruction algorithm with the variable `fudge` set to +8 results in the recirculation parameters shown on the left in Fig. 9 and with -8 on the right. We see that on the left the phase can be made constant at the expense of a larger variation of the gain, when comparing with the plot in the middle left of Fig. 8. In the plot on the right of Fig. 9 the gain can be made flat by changing the sign of the `fudge` parameter.

We conclude that the non-linearity does affect the reconstructed recirculation parameters and a careful calibration of the detectors should be done in order to avoid ambiguities.

5 Software

In order to facilitate the analysis of pulses we wrote a matlab user interface from which one can navigate to the data files, load the files, and perform the analysis. A screenshot is displayed in Fig. 10. The buttons at the top right are used to perform the standard actions

- **Load File** loads the data file. Here data files in .csv and .mat format are supported. If .csv files are requested, only the BPM file should be selected, the RF file will be automatically loaded as well. Once the data are loaded the BPM and RF trace are displayed in the top left frame and the IQ data just below. The non-linearity fudge alluded to above can then be applied to the IQ data by entering the fudge value to the input field at the lower left and pressing the `Fudge` button at the bottom part of the panel.

- **Synchronize** performs the fit of the RF profile to the model with *constant* recirculation gain and phase from Ref. [1]. Since the time shift is part of the fitting routine this information is used to adjust the timing of the BPM to be consistent with the RF power pulse. The top left plot is subsequently replaced by one showing the shifted BPM pulse, the RF pulse and the fit. Note that the BPM timing also can be adjusted manually by entering a single value in the Input field at the lower left of the panel and pressing **BPM shift**. This will manually displace the BPM pulse in time. In particular for pulses with breakdown this option is preferred to the automatic adjustment with the **Synchronize** button.

- **Analyze** then performs the analysis discussed in previous sections of this report. In the process the plots with the χ^2 data corresponding to Fig. 3 are shown in the top right of the software panel. The fit results for the coupling a and phase ψ are shown immediately below and the recirculation gain and phase as a function of time in the two graphs at the lower left. At the lower right the reconstructed I-Q

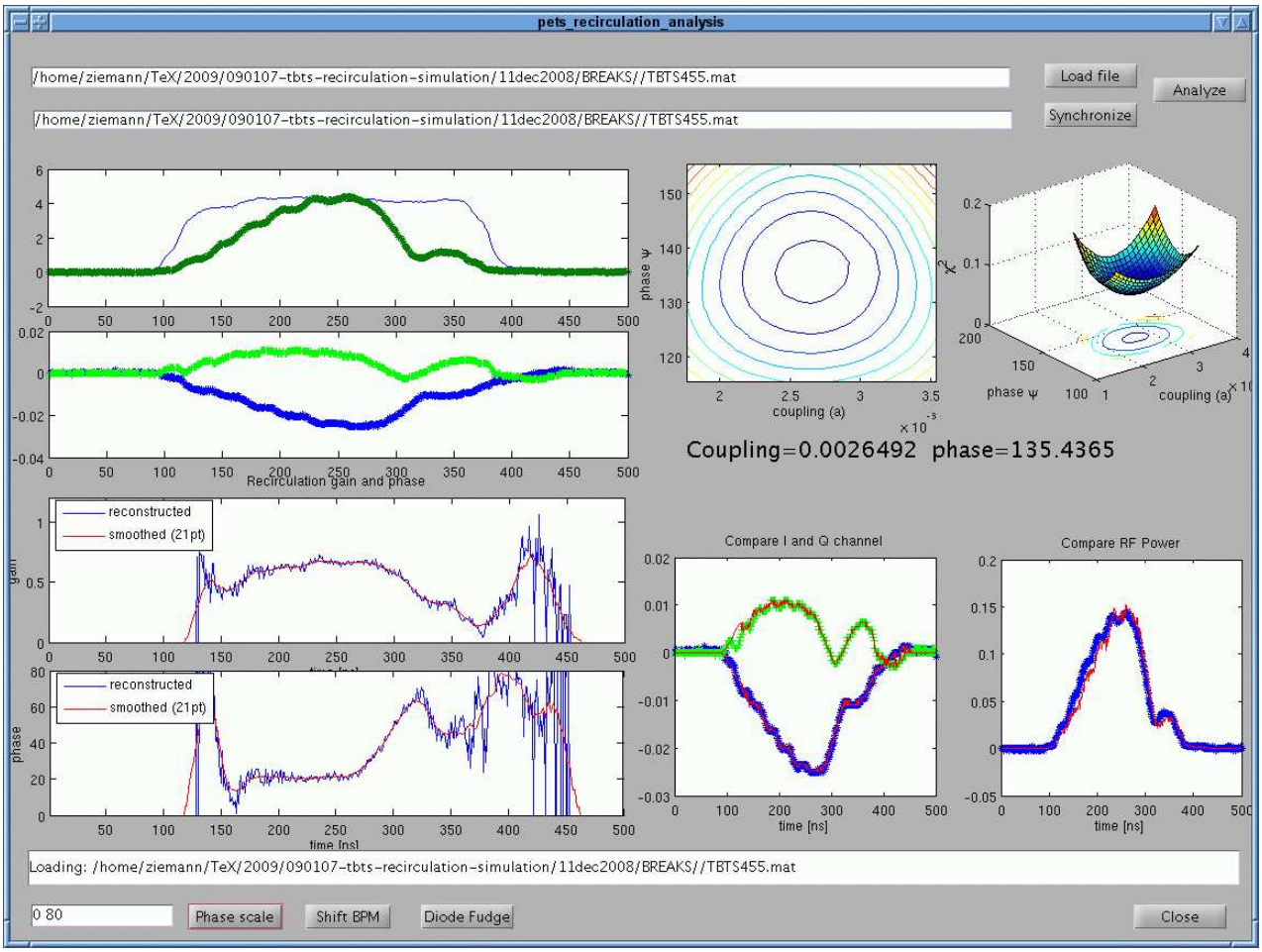

Figure 10: Screenshot of the integrated analysis software investigating a pulse where a breakdown occured just after 250 ns.

and RF power data (red trace) are compared with the original data. The vertical scale on which the recirculation phase is displayed can be adjusted manually by entering the desired minimum and maximum phase values in the input field at the lower left of the panel and pressing the button **Phase scale**.

Using this panel it is quite convenient to analyze a larger number of data files and get an impression how the different parameters vary.

6 Breakdown

We used the program to analyze a pulse that obviously displays a shortened RF power pulse that we interpret as a breakdown having occured. Such a pulse, labeled `BREAKS/TBTS455.mat` is shown in Fig. 10. Here the BPM timing was adjusted manually with the

Shift BPM button in such a way that the BPM pulse starts immediately before the RF power pulse in the top left graph. No non-linearity fudge is applied in this case. Then we press the **Analyze** button and obtain the result shown in Fig. 10. Here we note that the recirculation gain and phase are reasonably constant during the initial part of the pulse up to about 250 ns but then the gain starts to drop and the phase is rising linearly.

One might conjecture that during the breakdown a plasma is generated with free electrons that will absorb part of the RF power, thus leading to reduced gain. Moreover, the free electrons will change the dielectric properties of the space the RF power travels through and therefore the refractive index, which will induce a phase shift. Deducing the plasma density from the observed gain droop and phase shift is, however, referred to another report.

7 Conclusions

We developed an algorithm to determine the coupling of the beam to the RF in the PETS structure and the a-priory unknown phase between the PETS and IQ detectors together with the variation of the recirculation gain and phase along the pulse. We suspect, however, that part of the variation of the recirculation parameters is due to non-linearities in the IQ detectors, which needs to be investigated in the future. Otherwise the algorithm appears quite stable and can be used to study parameter variations under controlled changes of, for example, the position of the beam in the PETS. The most interesting feature, however, is the ability to investigate significant variations of the recirculation gain and phase along the pulse.

We also investigated a data set that exhibited signs of breakdown and found that the recirculation gain drops and the phase varies linearly after the discharge.

Stimulating discussions and support with the data acquisition by Roger Ruber and Erik Adli are gratefully acknowledged.

References

[1] R. Ruber, V. Ziemann, *An analytical model for PETS recirculation,* CTF3-note-092, March 2009.

[2] I. Syratchev, G. Riddone, S. Tantawi, *CLIC RF High Power production Testing Program,* Proceedings of the European Particle Accelerator Conference EPAC08 in Genoa, June 2008.

[3] I. Syratchev, *PETS and drive beam development for CLIC,* presented at the X-band RF structure and beam dynamics workshop in Daresbury, December 2008.

[4] E. Adli, presentation at the CTF3 technical collaboration meeting in January 2009.

[5] `http://www.mathworks.com`